Applied Thermal Engineering 219 (2023) 119425

Contents lists available at ScienceDirect

Applied Thermal Engineering

journal homepage: www.elsevier.com/locate/apthermeng

Research Paper

Numerical investigation of an oil-free liquid-injected screw compressor with ammonia-water as refrigerant for high temperature heat pump applications

Marcel Ulrich Ahrens [a,*], Ignat Tolstorebrov [a], Even Kristian Tønsberg [a], Armin Hafner [a], R.Z. Wang [b], Trygve Magne Eikevik [a]

[a] NTNU, Department of Energy and Process Engineering, Kolbjørn Hejes vei 1B, 7491 Trondheim, Norway
[b] SJTU, Institute of Refrigeration and Cryogenics, Shanghai Jiao Tong University, 200240 Shanghai, China

ARTICLE INFO

Keywords:
Modelica modeling
Liquid injection
Oil-free screw compressor
Ammonia-water mixture
Absorption-compression heat pump
High temperature heat pump

ABSTRACT

This study investigates a numerical model of an oil-free twin screw compressor with an ammonia-water mixture as refrigerant and liquid injection. The compressor was identified as the main constraint to increase the heat sink temperature of absorption-compression heat pump systems past 120 °C. Liquid injection can reduce the superheating of the vapor during compression, while an existing liquid film can provide lubrication and sealing, enabling oil-free operation. A quasi-one-dimensional numerical model was developed using the Modelica language. It considers the effects of liquid injection flows and injection positions, leakages, heat losses, and variation in ammonia mass fractions. The results revealed a strong influence of occurring internal leakages, varying ammonia mass fractions of the injected solution and changing injection flows and positions on the evolution of temperature, pressure, and compression power. The injection with a lower ammonia mass fraction is beneficial for reducing the discharge temperature, discharge pressure and compression power. The increase in injection flow led to a further reduction in the values obtained. Continuous wet compression, required for sufficient sealing and lubrication of the compressor, was achieved with injection at 360° at the beginning of the compression phase and an injection rate of about 10% of the compressor's suction mass flow. By distributing the injection to two injection ports, wet compression can be supported and occurring under-compression and backflow can be reduced.

1. Introduction

Thermal processes in the industry are responsible for increasing energy consumption and the associated CO_2 emissions [1]. It is therefore of great interest to improve the energy efficiency of heat supply systems to reduce the consumption of energy and resources [2]. At the same time, large amounts of low-grade waste heat are available for potential waste heat recovery in various industrial processes [3]. For example, the waste heat potential in the EU is estimated at approx. 300 TWh/year, of which one third is at the temperature level below 200 °C, often referred to as low-temperature waste heat [4]. The use of high temperature heat pumps with natural working fluids, such as ammonia and water, instead of conventional boilers is an effective measure to exploit available waste heat while reducing the consumption of energy and dependency of fossil fuels, as outlined by Bergamini et al. [5] in a thermodynamic system comparison. Ahrens et al. [6] supported this statement by presenting operational performance results of an integrated energy system of an existing dairy plant, using heat pumps entirely for all cooling and heating applications. Many authors such as Arpagaus et al. [7], Kosmadakis [8], Marina et al. [9], and Jiang et al. [10] investigated and summarized the possibilities of using high temperature heat pumps and found great potential for the application in various industrial sectors for the supply of process heat with sink temperatures above 100 °C.

One of the suitable heat pump solutions for various industrial high temperature applications is the absorption-compression heat pump (ACHP) system with the zeotropic ammonia-water mixture as working fluid. The ACHP system combines the advantages of achievable sink temperatures up to 120 °C with large temperature lifts (>60 K) and non-isothermal heat transfers (>30 K) [11]. To increase the system efficiency and further extend the range of applications by achieving higher sink outlet temperatures and associated pressure levels, the compressor was

* Corresponding author.
E-mail address: marcel.u.ahrens@ntnu.no (M.U. Ahrens).

https://doi.org/10.1016/j.applthermaleng.2022.119425
Received 2 June 2022; Received in revised form 24 August 2022; Accepted 28 September 2022
Available online 3 October 2022

Nomenclature

Abbreviations

ACHP	Absorption compression heat pump
CFD	Computational fluid dynamics
CV	Control volume
IHX	Internal heat exchanger

Roman Letters

A	Flow area [m^2]
f	Operational frequency [Hz]
h	Specific enthalpy [J/kg]
$\dot{m}$	Mass flow rate [kg/s]
p	Pressure [bar]
$\dot{Q}$	Heat transfer rate [W]
T	Temperature [°C]
u	Specific internal energy [J/kg]
V	Volume [m^3]
W	Work [J]
$\dot{W}$	Power [W]
x	Ammonia mass fraction [-]

Greek symbols

α	Heat transfer coefficient [W/m^2K]
θ	Rotational angle of male rotor [rad]
ν^i	Built-in volume ratio [-]
ρ	Density [kg/m^3]
ω	Angular velocity [rad/s]

Subscripts

body	Compressor body
comp	Compression
dis	Discharge
disp	Displacement
eff	Effective flow area
in	Inlet
inj	Injection
j	Index
leak	Leakage
lean	Lean solution
max	Maximum
out	Outlet
rich	Rich solution
suc	Suction

identified as the main constraint due to limitations in the manageable compressor discharge temperature [12]. During his investigations, Zaytsev [13] identified the use of liquid-injected screw compressors (in operation as wet compression) as a potential solution to the problem of occurring superheat during the compression of ammonia vapor.

The general objectives of liquid injection during the compression process in a screw compressor include the reduction of occurring leakages along with the reduction of superheating, resulting in improved efficiency of the compressor [14]. Furthermore, this can lead to an oil-free operation of the ACHP system, promising further benefits including lower installation costs due to fewer components (oil separator and cooler) and higher efficiencies due to improved heat transfer and reduced heat losses without the use of oil. Given the elimination of oil stability issues in oil-free operation, an increased compressor discharge temperature can be accepted and exploited to potentially increase the achievable heat sink temperatures, as outlined by Infante Ferreira et al. [15]. Zaytsev et al. [16] stated that providing the compressor with sufficient liquid injection for lubrication and sealing is essential to increase the compressor's efficiencies and maintain the thermal limits of the compressor's material by providing cooling.

The process of liquid injection in twin screw compressors was investigated by several authors, both theoretical and experimental, for different refrigerants and working conditions. For the theoretical investigation, a variety of models with mostly numerical approaches were developed using different methods [17]. As reviewed by Wang et al. [18], these range from quasi-one-dimensional models to more complex computational fluid dynamics (CFD) models with varying degrees of complexity by incorporating different assumptions (homogenous or heterogenous model, losses considered, etc.) and phenomena occurring (heat and mass transfer). Stosic et al. [19] investigated the influence of oil injection and analysed widely the effects of various parameters such as oil flow rate, inlet temperature, droplet atomization, oil injection port position and compressor speed on the performance of a twin screw compressor. The authors concluded that the parameters have varying influences on the performance and an optimal oil injection quantity can be found. In another study of oil-free compressors, Stosic et al. [20] demonstrated that injecting small amounts of water to control the rotor temperature was sufficient to operate single-stage compressors at higher pressure ratios with only minor modifications required. Yang et al. [21] conducted an experimental investigation of a water-injected process-gas screw compressor and found that the liquid injection could reduce the compressor discharge temperature significantly while increasing the capacity. The authors further stated that an optimal mass flow of injected water exists to effectively lower the discharge temperature while sealing the gap between the female and male rotors. Tian et al. [22] investigated a water-injected twin-screw compressor for water vapor compression and demonstrated that the injection rate must be adjusted to the respective rotor speed and operating point. The aim is to achieve saturated discharge temperature and to avoid flooding with too much liquid water, as this results in the highest efficiencies. Furthermore, a uniform and fine atomization by using nozzles is advantageous, while the injection temperature revealed only little effect on the cooling effect. Basha et al. [23] numerically investigated the implementation of the oil injection for a twin screw compressor. They found that the distribution of the injection over multiple injection ports for the same total liquid quantity revealed a positive influence on the compression process and the parameter achieved. These findings were confirmed by Tian et al. [24] in an additional numerical investigation on mass and heat transfer in an ammonia oil-free twin-screw compressor with liquid injection. The obtained results indicated that the average droplet diameter of the injected liquid should be less than 100 μm to ensure a sufficient cooling effect and improve the performance of the compressor. Furthermore, an optimization method for the positioning of the injection nozzle and the amount of injected liquid was proposed. Based on their results, the authors recommended adding a second injection nozzle. This should be placed after the starting point of the compression process, where the temperature gradient is greatest, and should receive about 70 % of the total injected amount. Patel and Lakhera [25] conducted a comprehensive review of experimental studies related to twin screw compressors. They concluded that for oil-free operation the understanding of improved thermal management through the usage of liquid injection along with self-lubricated bearings must be further explored.

The conducted literature review revealed that many investigations were performed on liquid injection in twin screw compressors using pure refrigerants and oil injection. It was stated that liquid injection had an overall positive influence on the achievable efficiency and the reduction of superheating. Thereby, it is important to maintain a high vapor quality of the compressed fluid while avoiding the flooding of the compressor with too much liquid. This results in an optimization

problem for the liquid injection flow. For the implementation of the injection, both the positioning of the injection port in the compression cycle and the distribution over a single port or multiple port injection revealed impact on the compression process. Furthermore, improved cooling effects were obtained with smaller droplet diameters, which can be provided by using nozzles and other devices.

Recent studies on the oil-free operation of the screw compressor and the use of ammonia-water mixture are limited to the conducted studies on wet compression with liquid injection in the suction and compression phases investigated by Gudjonsdottir et al. [26] and Gudjonsdottir and Infante Ferreira [27]. However, the system setup used, as well as the operating conditions investigated, deviate from the envisaged objectives of this study. Thus, a research gap exists for the planned integration of an oil-free twin screw compressor with liquid injection into the ACHP system at high temperature operation. For this, the effects on the compression process of different injected liquid rates, injection positions and injection distributions for changing ammonia mass fractions of the ammonia-water mixture must be investigated.

To address the identified research questions, this study introduces and investigates the quasi-one-dimensional model of an oil-free liquid-injected twin screw compressor for use in the ACHP system at high temperature operation. The purpose is to improve the understanding of the thermodynamic behaviour and expected results during the compression process with varying liquid injection parameters. Furthermore, the obtained results provide information for the preferred design of the liquid injection when integrated into ACHP systems and support the planning of necessary experimental investigations.

2. Background

In this section, the theoretical background for the conducted research is presented. First, the ACHP system using ammonia-water mixture as working fluid is described, with a special focus on the compressor to be investigated and the discussion of possibilities for implementing liquid injection. The subsequent thermodynamic analysis provides the basis for the development of the simulation model and the evaluation and assessment of the achieved results.

2.1. The absorption-compression heat pump system

A schematic illustration of the ACHP system, often referred to as Osenbrück cycle in recognition of its inventor Osenbrück (1895) [28], is presented in Fig. 1. For the focus of this study, two possible options for the desired implementation of liquid injection in the screw compressor under investigation were identified: injection of lean solution (Option 1) and injection of rich solution (Option 2).

In the ACHP, the desorber and absorber transfer heat with the heat source and sink. The ammonia-rich solution enters the desorber at low pressure (10). As the temperature increases, the solubility of the ammonia in water decreases, causing ammonia vapor to expel. As a result, a two-phase mixture leaving the desorber towards the liquid–vapor separator (1). The low-pressure vapor and lean solution are separated in the liquid–vapor separator before being directed to the compressor (2) and solution pump (4). The compressor increases the pressure and temperature of the vapor (2 to 3), while the pump elevates the pressure of the lean solution correspondingly (4 to 5). To improve the cycle performance, an internal heat exchanger (IHX) is installed to interconnect the solution streams. Heat is exchanged between the lean and rich solution, resulting in a temperature increase of the lean solution (5 to 6) and a decrease of the rich solution (8 to 9). At the high-pressure side, the lean solution (6) is then mixed with the superheated NH_3 vapor from the compressor (3) at the inlet of the absorber (7). In the absorber, vapor is absorbed by the liquid and the generated heat is transferred to the heat sink fluid. During the absorption process, the NH_3 mass fraction in the solution phase gradually increases and a saturated solution emerges at the outlet of the absorber. The ammonia-rich solution then flows through the IHX before being throttled down to desorber's pressure (8 to 9 to 10) and thus completing the cycle.

2.2. Possibilities for liquid injection

For the study of compression with liquid injection, the effects with varying NH_3 mass fraction of the injected solution (x_{inj}), injected mass flow rate $\left(\dot{m}_{inj}\right)$ and position of injection (θ_{inj}) are investigated. With respect to the structure of the ACHP system (see Fig. 1), two possible options for the arrangement of the injection line are highlighted. Option

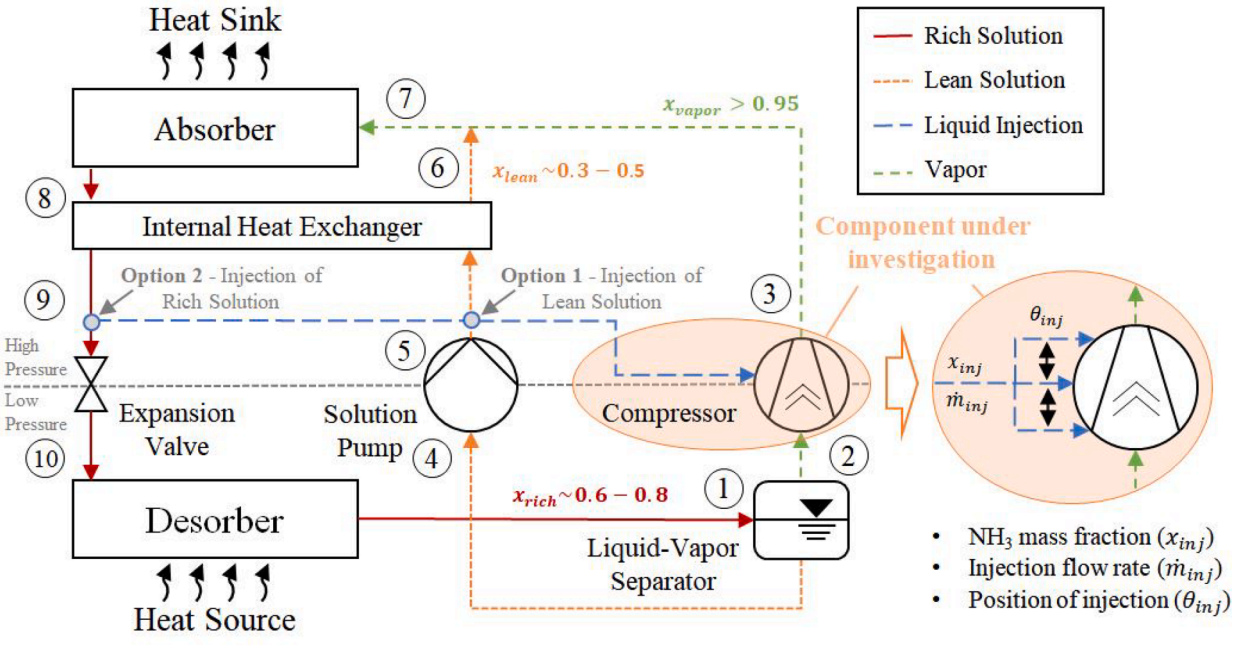

Fig. 1. Schematic illustration of ACHP system including possible liquid injection options.

1 - Injection of the lean solution: extraction of the lean solution (x_{lean} 0.3 −0.5) downstream of the solution pump, where the solution is significantly subcooled due to the previous pressure rise from the saturated state. Option 2 - Injection of the rich solution: extraction of the rich solution (x_{rich} 0.6 −0.8) downstream of the IHX and upstream of the expansion valve. In this case, the solution remains at high pressure and was subcooled by the lean solution. Thus, the solution for injection will be present in highly subcooled liquid state for both options. Depending on the position of the injection, subcooled solution will be injected into increasingly superheated vapor with the start of the compression phase. In this case, the solution is not in a state of equilibrium in terms of pressure and temperature. The equilibrium state of the solution parameters is strongly influenced by the injection flow rate and possibility of injection at multiple positions between suction, compression, and discharge phases, along with internal flows due to leakage. Furthermore, the thermodynamic properties of the solution and vapor phases change as a function of temperature, pressure, and NH_3 mass fraction. It is therefore important to further describe and analyse the expected thermodynamic behaviour of the NH_3-H_2O mixture during occurring parameter changes.

2.3. Thermodynamic analysis

The NH_3-H_2O mixture used in the ACHP system is a zeotropic mixture consisting of two solution components with different boiling points [29]. Fig. 2 shows the temperature-NH_3 mass fraction (T −x) diagram with bubble point and dew point lines at different pressure levels.

The indicated example is valid for liquid–vapor equilibrium conditions and illustrates the thermodynamic behaviour of the NH_3-H_2O mixture at a constant NH_3 mass fraction x_1 of 0.5 and pressure p_1 of 5 bar during the temperature change from subcooled solution state (0) to superheated vapor state (4). The injected solution (lean or rich) is in the subcooled state (0). The temperature of the solution is gradually increased due to the contact with the superheated vapor in compressor. At the boiling point ($1'$) the saturated vapor of NH_3 and H_2O is formed ($1''$). The further increasing of the solution's temperature (2) results in desorption of NH_3 and the NH_3 mass fraction in the liquid phase drops ($1'-3'$), while vapor fraction of NH_3 is increasing ($1''-3''$). In the superheated state (4) is the solution fully evaporated. Rising the pressure (p_1 to p_3) leads to increasing temperatures of the bubble point and dew point lines. Thus, the degree of subcooling of the solution at a higher pressure is increasing. It should be noted that the equilibrium state of the solution is not defined by pressure and temperature only. The significant amount of NH_3 in the superheated vapor shifts the equilibrium state of the NH_3-H_2O vapor mixture. Thus, the evaporation of saturated solution will continue to compensate for the low partial pressure of H_2O vapor in the gas mixture [24]. Due to this, in the case of low mass flow rates of the injected solution, the full evaporation will occur irrespectively on the temperature and pressure. When used in ACHP systems, however, remaining liquid and wet compression are essential for sufficient sealing and lubrication of the compressor.

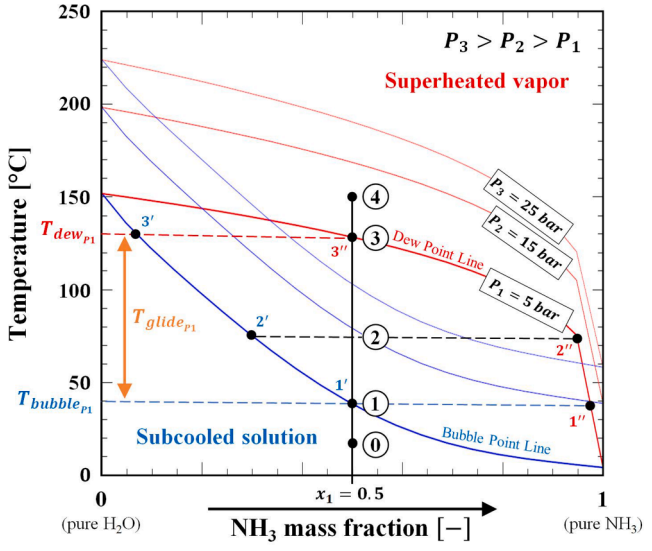

Fig. 2. Temperature-NH_3 mass fraction (*T*-x) diagram with bubble point and dew point lines for NH_3-H_2O mixture at different pressure levels.

3. MODELICA twin screw compressor model

The developed model of the oil-free liquid-injected twin screw compressor is a quasi-one-dimensional numerical model with multiple control volumes (CV), each representing the volume of one rotor cavity, and follows the concepts presented by Chamoun et al. [30] and Tian et al. [22]. The model was written in the object-oriented Modelica language [Modelica Association] and was implemented and solved in the Dymola 2020 simulation environment using the ESDIRK23A standard solver by Dassault Systèmes [31]. Two commercial Modelica libraries were used for the implementation, namely TIL-Suite 3.5 and TILMedia 3.5 provided by TLK-Thermo GmbH [32,33]. TIL-Suite is a component library for steady-state and transient simulation of thermodynamic systems, while TILMedia provides methods and data for calculating the properties of thermophysical substances. The model considers the effects of liquid injection, leakage flows, and heat losses and is designed to investigate various arrangements of liquid injection and operating conditions.

3.1. Description of the control volume

The change in the boundaries (volume) of each CV occurs with time, often expressed as rotational angle of the male rotor. Thereby, the total rotation time/angle that one cavity undergoes during a complete compression cycle depends on the length and pitch of the rotors. This is applied from the beginning of the suction phase to the end of the discharge phase. When a CV enters the suction phase its volume increases, while it decreases during the compression and discharge phases. The underlying volume alteration throughout an entire compression cycle is defined by the compressor's geometry. This is identical for all CVs but contains a time delay between individual CV. Thus, the leading cavity (e.g., CV_j) can simultaneously undergo a volume reduction, while the trailing cavity (CV_{j-1}) still undergoes a volume increase. Each CV is an open system with three inlet paths (suction, leak-in and liquid injection) and two outlet paths (discharge and leak-out). Additionally, the system receives compression power from the rotor ($\dot{W}_{comp}$) and dissipates heat to the compressor body and ambient ($\dot{Q}_{loss}$). As a result, pressure, temperature, mass, internal energy and NH_3 mass fraction differ in each CV at any point in time. Fig. 3 illustrates the simplified mass and energy balance associated with each CV.

3.2. Basic equations for the control volume

Based on a set of differential equations for the conservation of mass and energy, the model simulates the processes (heat and mass flow) of the twin screw compressor in each CV at any time. Since there are leakage flows and the cavities are periodically connected to suction, injection and discharge, the CV is treated as an open system which can be described by the first law of thermodynamics [35]. Neglecting kinetic energy and gravitational energy, and expressing the equations based on rotational angle of the male rotor (θ), the mass and energy balances can be expressed as [36,37]:

$$\frac{d(m)}{d\theta} = \sum \frac{dm_{in}}{d\theta} - \sum \frac{dm_{out}}{d\theta} \quad (1)$$

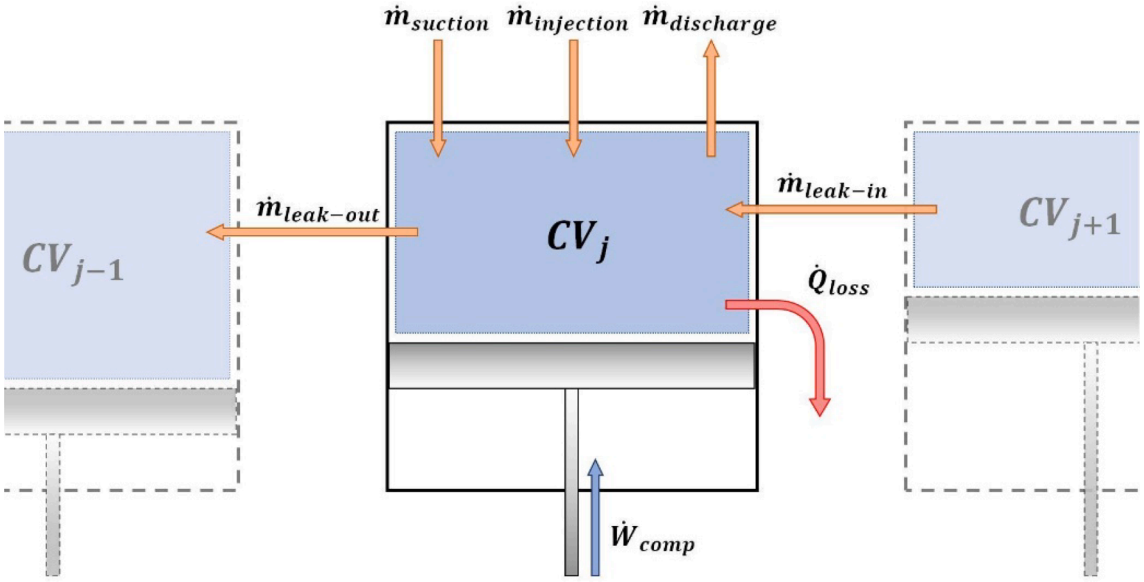

Fig. 3. Simplified mass and energy balance associated with each control volume ().
adapted from [34]

$$\frac{d(mx)}{d\theta} = \sum \frac{dm_{in}}{d\theta} x_{in} - \sum \frac{dm_{out}}{d\theta} x_{out} \tag{2}$$

$$\frac{d(mu)}{d\theta} = \sum \frac{dm_{in}}{d\theta} h_{in} - \sum \frac{dm_{out}}{d\theta} h_{out} + \frac{dW_{comp}}{d\theta} - \frac{dQ_{loss}}{d\theta} \tag{3}$$

where m is mass, x is NH_3 mass fraction, u is specific internal energy, h is specific enthalpy, W is compression work and Q is heat between the working fluid and compressor body. As the working fluid is a mixture, Eq. (2) is required in addition to Eq. (1) to determine the composition of the mixture. At an angular velocity of $\omega = d\theta/dt$, the equations can be formulated as [30]:

$$\omega \frac{d(m)}{d\theta} = \sum \dot{m}_{in} - \sum \dot{m}_{out} \tag{4}$$

$$\omega \frac{d(mx)}{d\theta} = \sum \dot{m}_{in} x_{in} - \sum \dot{m}_{out} x_{out} \tag{5}$$

$$\omega \frac{d(mu)}{d\theta} = \sum \dot{m}_{in} h_{in} - \sum \dot{m}_{out} h_{out} + \dot{W}_{comp} - \dot{Q}_{loss} \tag{6}$$

With the compression power expressed as:

$$\dot{W}_{comp} = -\omega p \frac{dV}{d\theta} = -p \frac{dV}{dt} \tag{7}$$

where p is pressure in the CV and dV/dt is the time derivative of the cavity volume. For this investigation, a mechanical efficiency of 100 % is assumed and friction losses as a function of the compression power and rotation speed are neglected. The temperature of the working fluid is substantially higher than the temperature of the ambient air surrounding the compressor. Therefore, heat losses to the compressor body and the ambient should be assessed. The heat transfer rate from the working fluid to the compressor body is determined as [38]:

$$\dot{Q}_{loss} = \alpha V^{2/3} (T - T_{body}) \tag{8}$$

Where α is the heat transfer coefficient between working fluid and compressor body, $V^{2/3}$ denotes the available heat transfer area of the cavity volume, T is the temperature of the working fluid, and T_{body} is the average surface temperature of the compressor body. Determining the temperature of the compressor body is not trivial and is generally influenced by the heat transferred by the working fluid and additional factors such as mechanical heat losses. The temperature of the working fluid and the influence of other factors vary greatly along the length of the compressor during the compression process. However, the thermal conductivity of the compressor body made of steel is relatively high, and uniform temperature distribution can be simplified assumed.

3.3. Determination of thermodynamic state properties

By solving the mass and energy equations, the pressure, specific internal energy, and NH_3 mass fraction of the NH_3-H_2O mixture are determined for each CV throughout the entire compression cycle continuously. With the assumption of liquid vapor equilibrium conditions, the thermodynamic state properties of the NH_3-H_2O mixture in each CV were determined using the calculation procedures provided by the TILMedia library [33]. Here, pressure, specific enthalpy and NH_3 mass fraction are used as input parameters. By using the specific internal energy calculated from Eq. (6), the specific enthalpy in the CV can be obtained:

$$h = u + \frac{p}{\rho} \tag{9}$$

where ρ is the density of the working fluid. The density is obtained from the TILMedia property calculation procedure [33] and with $m = \rho V$ also utilized when calculating the total mass in the CV.

3.4. Determination of flow rates

As illustrated in Fig. 3, there are different paths through which the working fluid can flow throughout an entire compression cycle. The mass flow rates for the suction, discharge and leakage paths are determined using [39]:

$$\dot{m} = A_{eff} \bullet \sqrt{2 \bullet \rho \bullet \Delta p} \tag{10}$$

where A_{eff} is the effective flow area of the flow path in m^2, ρ is the density of the working fluid upstream of the flow, and Δp is the pressure difference across the flow area. When calculating suction mass flow rates, for instance, A_{eff} represents the effective flow area of the suction port, ρ the density of the working fluid in the suction line, and Δp the pressure difference between the suction line and the connected CV. Thereby, A_{eff} varies with time as the CV goes through the suction phase, while it is set to zero during the compression and discharge phases. The same applies adjusted for the discharge path and phase. The

characteristics of the A_{eff} curves are dependent on the set built-in volume ratio (V^i) and are defined by the geometry of the respective ports and the rotor profile [40]. Contrary to the other paths, the injection mass flow rate is defined as a fixed value. The injection starts when a CV reaches the injection port location (θ_{inj}). It remains active until the trailing cavity reaches the injection port location, determined by the existing phase shift between the CVs.

Occurring leakage flows within the compressor are considered by linking adjacent CVs. The leakage path represents the gap between the rotor tips and the compressor housing, as it is one of the paths with the greatest impact on compressor performance [41]. Here, A_{eff} depends on the length of the sealing line, and it is assumed to be directly proportional to the cavity volume. Furthermore, it is assumed that the length of the sealing line between two adjacent CVs is determined by the smallest cavity volume at each point in time. Thus, the effective leakage area is calculated using the leakage area function as follows:

$$A_{eff,leak} = C_{leak} \bullet \min\left(V_{CV_{j-1}}, V_{CV_j}\right) \quad (11)$$

where C_{leak} represents the leakage flow coefficient, an estimated constant ranging from 0 to 1 [m^{-1}]. $V_{CV_{j-1}}$ and V_{CV_j} represent the adjacent trailing and leading cavity volumes behind and in front of the sealing line.

3.5. Model parameter

To perform the simulations in this investigation, the model input parameters listed in Table 1 were used to define the screw compressor model.

The compressor model is divided into eight control volumes, resulting in a phase shift of 90° between each CV. It is assumed that for each CV the total rotation angle during a compression cycle (θ_{cycle}) is 720°. Under the assumption that the male rotor spins at an operational frequency (f) of 50 Hz, it takes 40 ms to complete one entire cycle. The displacement volume (V_{disp}) is set to 335 cm^3 with a $\nu^i = (V_{disp}/V_{dis})$ of 3.65. The maximum effective flow areas are set at 50 cm^2 for the suction path (A_{suc}) and 10 cm^2 for the discharge path (A_{dis}). Fig. 4 shows the volume evolutions for two adjacent CVs with 90° phase shift and the resulting effective flow area $A_{eff,leak}$ of the leakage path through the gap between rotor tips and compressor housing using Eq. (11) with a C_{leak} value of 0.05 m^{-1}.

The evolution of the effective flow area A_{eff} depends on the smallest volume of the adjacent CVs. While one of the CVs remains in the compression phase (from V_{disp} to V_{dis}) starting from state (1) and ending at state (2), an effective flow area exists, and leakage flow occurs. If both CVs are in the suction phase (from 0 to V_{disp}) or discharge phase (from V_{dis} to 0), the respective path openings represent a much larger area, and the leakage area is set to zero. The same applies when the leading CV (CV_j) enters the suction phase, since the CVs are on opposite sides of the compressor and there is no leakage connection between them.

3.6. Simulation setup

The developed screw compressor model can be used as a stand-alone model or integrated into a larger system model. For this study, the model was used as stand-alone and connected with boundaries defining the conditions for suction, injection, and discharge ports. Each boundary is defined by three parameters: pressure, temperature and NH_3 mass fraction. Fig. 5 illustrates the simulation setup with the defined boundary conditions for the suction, injection, and discharge ports.

Table 1
Model input parameter used.

Parameter	# of CV	θ_{cycle}	f	V_{disp}	ν^i	A_{suc}	A_{dis}
Value	8	720°	50 Hz	335 cm^3	3.65	50 cm^2	10 cm^2

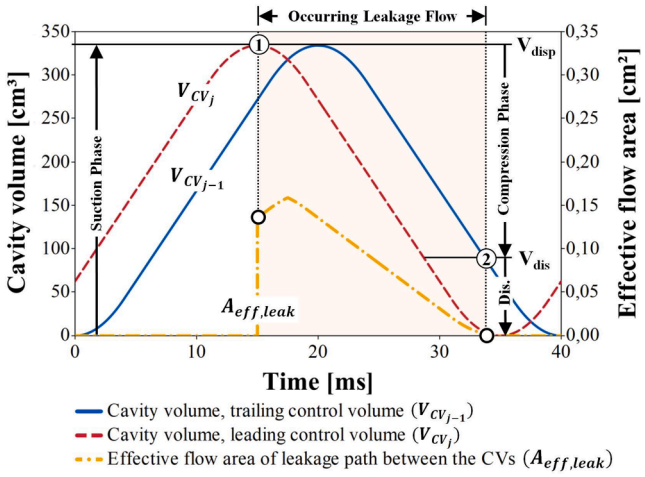

Fig. 4. Evolution of cavity volumes of two adjacent CVs and resulting effective flow area of the implemented leakage path through the gap between rotor tips and compressor housing.

The defined boundary conditions are based on the expected operating conditions for the screw compressor in the ACHP system (see Section 2). The desorber and absorber pressures are assumed to be 5 bar and 25 bar, respectively, corresponding to the suction (p_{suc}) and discharge (p_{dis}) pressure of the compressor model. The NH_3 mass fraction of the rich solution is set to 0.7 with a temperature of 55 °C in the liquid–vapor separator. In liquid–vapor equilibrium, this results in the NH_3 mass fraction of 0.985 in the vapor phase (x_{suc}). The injection boundary pressure, p_{inj}, is set to the high-pressure side of 25 bar and the injection temperature, T_{inj}, to 55 °C. During injection, an adjustment with the prevailing pressure in the CV takes place. Thus, the injection pressure at the respective injection port is adjusted depending on the positioning. The NH_3 mass fraction of the injected liquid, x_{inj}, is defined as variable (var.) since simulations with varying values are to be performed. The values for T_{dis} and x_{dis} of the discharge boundary are the result of the compression in the compressor model. In addition to the model input parameters given in Table 1, values for C_{leak}, the injection angle (θ_{inj}) and the injection mass flow rate ($\dot{m}_{inj}$) were defined and varied to perform the simulations.

3.7. Model validation

The purpose of the present study is to improve and discuss the understanding of the thermodynamic behaviour of an oil-free twin-screw compressor with NH_3-H_2O mixture as refrigerant and liquid injection during the compression process. Achievable efficiencies and other performance parameters are influenced by occurring leakages, mechanical losses, and heat losses, and other component and/or operation specific parameters. These are difficult to predict without detailed data on the geometry and operational performance and require experimental investigations. Since this study is a preliminary theoretical investigation without an existing prototype and detailed experimental data for validation, a component-based validation is performed to verify the reliability of the achievable results.

For this, the component models used in the developed model are checked and validated with respect to their physical and thermodynamic properties and reliability. The TILMedia 3.5 library [33] provides the determined thermo-physical properties of the investigated NH_3-H_2O mixture for each time point. The operating parameters are within the valid working range and can therefore be assumed to be sufficiently accurate. Further, TIL-Suite 3.5 [33] model components such as ports were utilized, which are commonly used and provide reliable results. Smitt et al. [42] used these libraries for a variety of components to study integrated energy systems and obtained less than 10 % deviation from

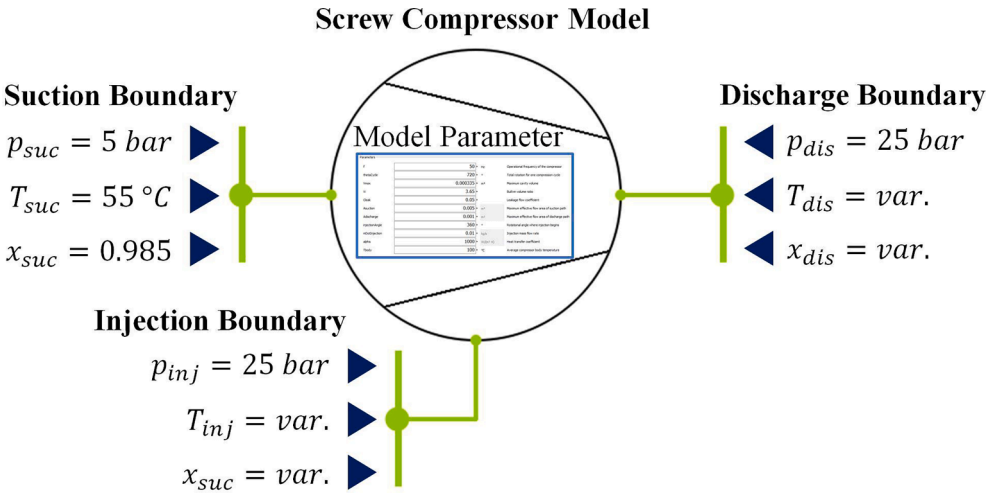

Fig. 5. Simulation setup of the screw compressor model with defined boundary conditions.

the experimentally determined readings. Chamoun et al. [30] used a Modelica-based model for the comprehensive analysis of an experimentally tested twin screw compressor. Although no explicit validation of the model results was performed, it can be assumed that the deviation of the simulation results was within an acceptable range.

Occurring flow rates are implemented using Eq. (10), which is widely used for investigations of this phenomena in screw compressors [38,39]. Required area functions for inlet and outlet ports in this study are defined following the extensive investigation by Zaytsev [13]. The same applies to the implemented leakage flows, which are calculated using Eq. (11). The curves of the cavity volume and the resulting effective flow area are shown in Fig. 4 and are comparable to the results presented by Zaytsev [13]. For the implemented control volume, homogeneous pressure and liquid–vapor distribution are assumed, and mechanical losses are neglected. With these assumptions, the compression process in the CV can be compared with isentropic compression and for a case without leakage and liquid injection compared with adiabatic compression. In this context, the obtained results are presented and discussed in the next section.

4. Results and discussion

The aim of this study was to investigate the effects of different parameters on the compressor's discharge temperature and pressure, and compression power throughout the compression process. The discharge temperature of the compressor was identified as the main constraint for the ACHP system in achieving higher heat sink temperatures and system efficiency. For this, the examined results focus on one control volume passing through an entire compression cycle.

4.1. Leakage flow coefficient

Internal leakage influences the performance of screw compressors [13,41]. It is therefore essential to apply an appropriate value for the leakage flow coefficient, C_{leak}, in the model. Simulations were performed with varying C_{leak} values ranging from 0 m^{-1} to 0.1 m^{-1} without liquid injection ($\dot{m}_{inj}$ set to 0). Fig. 6 presents the resulting pressure evolution throughout a whole compression cycle of a CV in a pressure–volume diagram.

The pressure curves indicate that increasing C_{leak} values accelerate the pressure evolution, as reflected by higher pressures at a respective volume. Moreover, it results in higher degree of over-compression at the end of the compression phase when reaching the discharge port and increases the required compression power. With further increasing of leakage ($C_{leak} > 0.1\ m^{-1}$), over-compression is decreasing and even

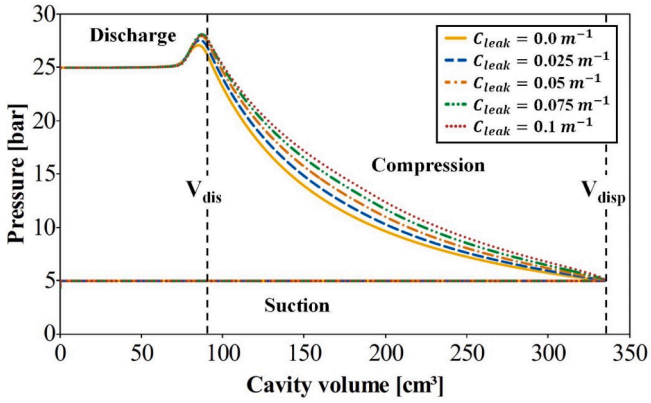

Fig. 6. Pressure-volume diagram for different C_{leak} values without liquid injection ($\dot{m}_{inj} = 0\ kg/s$).

under-compression can be observed, due to excessive backflow of working fluid at a fixed built-in volume ratio (not shown at Fig. 6). At the same time, high leakage increases the discharge temperatures, as heated vapor flows back from volume cavities at higher pressure levels towards the suction port and is partly re-compressed. The maximum temperature reached 243 °C at C_{leak} of 0.1 m^{-1}, and it was 40 K higher when compared with the ideal case without leakage. The pressure curve without leakage ($C_{leak} = 0.0\ m^{-1}$) and with no liquid injection can be used as a reference for adiabatic compression since other losses are neglected. The plotted curve patterns are qualitatively comparable with other literature results [15].

During the suction phase, leaking vapor occupies a fraction of the available suction volume, thus decreasing the volumetric efficiency occurs. With a C_{leak} value of 0.1 m^{-1}, the reduction in volumetric efficiency was calculated at 13 %. Fleming and Tang (1995) [41] stated that the implemented leakage path between the rotor tips and the compressor housing contributes to a 2 % to 3 % reduction in volumetric efficiency compared to a scenario without leakage. An equivalent result can be obtained with a value of C_{leak} between 0.025 m^{-1} and 0.035 m^{-1}. However, to compensate for the additional reductions in volumetric efficiency caused by leakage paths other than those considered in the model, a C_{leak} value of 0.05 m^{-1} was used for the further investigation of liquid injection. This leads to a reduction in volumetric efficiency of about 5 % compared to the ideal case without leakage.

4.2. Heat losses to compressor body and ambient

The temperature of the working fluid in the CV rises significantly during the compression process, similar to the increase in pressure (see Fig. 6). Thus, there is a very large temperature difference between the working fluid and the ambient at the end of the compression phase, implying that large heat losses can occur. On the other hand, the volume of the compression cavity, and thus the available transfer area, decreases continuously towards the end of compression. These opposing trends lead to uncertainties on whether the heat losses to the compressor body and ambient have a significant impact on the compression parameters. It is often argued in the literature that the heat loss to the casing and the environment can be neglected because the heat transfer coefficient between the steam and the compressor casing is small [20]. Tian et al. [22], in their investigation of water-injected screw compressors, further specified that the cooling effect of the injected liquid has greater influence and heat losses to the ambient are neglected.

To evaluate the effects of heat losses to the compressor body and ambient, an investigation was performed for a case without liquid injection ($\dot{m}_{inj}$ set to 0) and a C_{leak} value of 0.05 m^{-1}, assuming a uniform T_{body} value of 80 °C and a varying α value from 0 up to an unlikely high value of 5000 W/m^2K. The achieved results revealed that the influence of heat losses is minimal, even with an unreasonably high value for α, such as 5000 W/m^2K. The working fluid is slightly heated during the suction phase, and there is a slight cooling effect on the last section during discharge, but apart from this the temperature curves are almost identical. The same results are obtained for pressure and compression work. Change rates are below ± 1.0 % for the observed maximum values. Furthermore, as described by Stosic et al. [20], the temperature profile in an actual screw compressor is not uniform during operation and the temperature of the compressor body is higher on the discharge end compared to the suction end. Thus, it can be argued that the temperature differences between the working fluid and the compressor body will be smaller, and less heat will be transferred than in the simulation when using an average body temperature. This strongly suggests that heat losses to the compressor body can be neglected in this study. Therefore, the α value is set to zero for the following simulations and heat losses are not considered.

4.3. NH_3 mass fraction of the injection liquid

The NH_3 mass fractions of the various streams in ACHP systems change depending on the design and operating conditions. To investigate the effects on the compression process, the NH_3 mass fraction of the injection liquid was varied from pure water ($x_{inj} = 0$) to pure ammonia ($x_{inj} = 1$) at a constant injection angle of 360° (beginning at the start of the compression phase and active for a rotational angle of 90°) and injection mass flow rate of 0.01 kg/s, corresponding to about 5 % of the

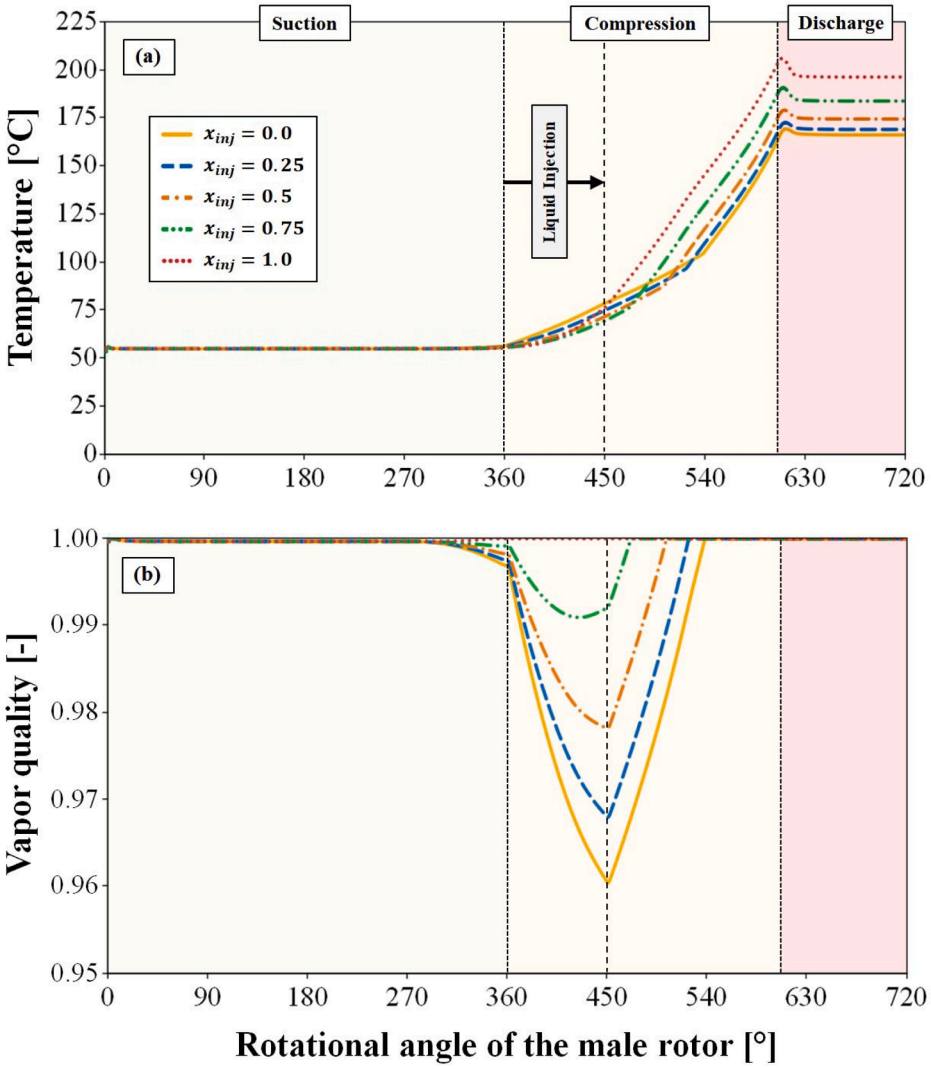

Fig. 7. (a) Temperature and (b) vapor quality evolution for different x_{inj} values at constant $C_{leak} = 0.05\ m^{-1}$, $\theta_{inj} = 360^{\circ}$ and $\dot{m}_{inj} = 0.01\ kg/s$.

compressor's suction mass flow rate. Fig. 7 illustrates the temperature and vapor quality evolution for different ammonia-water solutions.

The lowest discharge temperature was obtained when the injection liquid was pure water ($x_{inj} = 0$), while the highest discharge temperature was obtained for pure ammonia ($x_{inj} = 1$), Fig. 7a. Characteristics of the different curves were very similar, with a relatively low temperature rise during the first part of the compression phase. At a certain point, the gradient of the respective curve changes, and the temperature rises more sharply when the liquid fraction is fully evaporated. This inflection point occurred earlier for higher NH_3 mass fraction of the injection liquid, and it resulted in higher discharge temperature as well. This can be explained by increased evaporation of liquid and differences in heat capacity and saturation temperature for different NH_3 mass fractions of the ammonia-water mixture (see Fig. 2). Once the liquid injection stops and all remaining liquid is evaporated, the temperature increases sharply.

The plotted evolution of the vapor quality, Fig. 7b, helps to understand the temperature profile alteration shown on Fig. 7a. Except for pure ammonia, the vapor quality drops into the two-phase region when liquid is injected into the CV, but it immediately rises again after the injection stops and the volume is further compressed. The wet compression occurs in all such cases. The length of the wet compression strongly depends on the NH_3 mass fraction in the injected solution: the longest wet compression was observed for pure water and none for pure ammonia. The NH_3 mass fraction in the CV varies from 0.985 at suction and ranges between 0.941 and 0.987 at the discharge for pure water and ammonia, respectively. The extremums for temperature and pressure, and compression power are given in Table 2.

The highest temperature, pressure and compression power were observed when injecting pure ammonia. The high temperature is beneficial for oil-free high temperature heat pumps; however, it can be limited by the material properties of the compressor. At the same time, for the investigated case, where the pressure in absorber was set to 25 bar, the injection of pure ammonia resulted in the highest degree of over-compression, when compared with pure water. Due to this, an increased compression power was observed.

4.4. Injection mass flow rate

Previous results have indicated that remaining liquid in the CV (vapor quality less than 1) during the compression process influences the discharge temperature, degree of over-compression and compressor power. Therefore, it is expected that besides the NH_3 mass fraction, the injected mass flow rate has a significant influence on the compression process. In the further investigation, the NH_3 mass fraction of the injection fluid is set to 0.4 and 0.7, respectively, which are feasible values for the lean and rich solution in the ACHP system. The injection mass flow rate varied from 0.00 kg/s to 0.02 kg/s at a constant C_{leak} value of 0.05 m^{-1} and injection angle of 360°. This corresponded to a range between 0 % and 10 % of the compressor's suction mass flow rate. Fig. 8 shows the temperature evolution for different liquid injection mass flow rates with NH_3 mass fraction of 0.4.

The results indicate a significant influence of the injection mass flow rate on the temperature evolution and maximum discharge temperature. The discharge temperature is the highest with zero injection and decreases with higher injection mass flow rates. The inflection point of temperature evolution was observed when the liquid fraction was fully evaporated. This trend was similar with the findings from Fig. 7a. With higher injection rates, the inflection point shifts towards the end of the compression phase. At an injection mass flow rate of 0.02 kg/s, wet compression occurs during the entire compression phase. With increased NH_3 mass fraction of 0.7, complete wet compression occurs first at a value between 0.02 kg/s and 0.025 kg/s. The extremums for temperature and pressure, and compressor power for different injection mass flow rates with NH_3 mass fractions of 0.4 and 0.7 are given in Table 3.

Table 2
Results for different x_{inj} values at constant $C_{leak} = 0.05\ m^{-1}$, $\theta_{inj} = 360^{\circ}$ and $\dot{m}_{inj} = 0.01\ kg/s$.

x_{inj} [-]	0.0	0.25	0.5	0.75	1.0
T_{max} [°C]	169.2	172.6	179.2	191.2	207.3
p_{max} [bar]	25.82	25.96	26.24	26.85	27.65
$\dot{W}_{comp}$ [kW]	54.07	54.35	54.94	56.21	57.89

The discharge temperature was influenced by the injected mass flow rates and solution mass fraction. The lowest discharge temperature was observed for injected mass flow rates of 0.02 kg/s and lean solution with NH_3 mass fraction of 0.4. The injection of rich solution ($x_{inj} = 0.7$) shows the same trend as lean solution, but discharge temperature, pressure and compression power were higher. The discharge NH_3 mass fractions in the CV range from 0.985 to 0.937 and to 0.962 for injection mass flow rates from 0.0 kg/s to 0.02 kg/s with NH_3 mass fractions of 0.4 and 0.7, respectively. The increasing of the injected mass flows leads to under-compression within the CV when reaching the discharge port at a rotational angle of 605°. As shown in Fig. 9, this can result in backflow from the discharge port into the CV, generating pressure and flow pulsation.

Pressure and flow pulsation result in additional mechanical stress on the compressor and noise generation. To avoid over- or under-compression, an injection mass flow rate of approx. 0.01 kg/s for an NH_3 mass fraction of 0.4 is recommended. Here, only the leakage flow into the trailing CV was compensated, but no excessive backflow into the CV was generated. With an NH_3 mass fraction of 0.7, the recommended rate is between 0.01 kg/s and 0.015 kg/s. For application in the ACHP system, an optimization problem arises that must be solved depending on the specific operating conditions, considering all system parameters.

4.5. Positioning of injection ports

The influence of the position of the injection port was investigated. The injection angle (θ_{inj}) was set up at 360°, 405°, 450°, 495° and 540°. The injection mass flow rate was set to 0.01 kg/s with NH_3 mass fractions of 0.4 and 0.7. Fig. 10 shows the example of temperature evolution in relation to the injection angle.

The increasing of the injection angle resulted in the increasing of the discharge temperature, discharge pressure and required compression power. That was true for both lean and rich solutions. The injection is characterised by the change of slope of the temperature increasing. The model indicated that wet compression occurs when the solution is injected at 360° and 405°. For the injection at 360°, this is clearly indicated by the temperature line inflection shown in Fig. 10. Further increase of the injection angle did not show the presence of the liquid fraction (vapor quality = 1) except at the injection point. This happens due to the high degree of superheat at an injection angle over 405°. At the time, the cooling of the superheated gas before reaching the injection point was observed for all investigated cases. This was explained by the leakage of cooled gas towards the suction port. The injection mass flow rate of 0.01 kg/s at 360° and 405° did not provide wet compression for the whole length of the compressor, which means it is insufficient for good lubrication. The mass flow analysis revealed that the injection of 0.01 kg/s does not generate backflow from the discharge port into the compression chamber, and under-compression was not observed for both the lean and rich solutions, irrespectively on the injection angle.

Three different injection mass flow rates (0.01 kg/s, 0.015 kg/s and 0.02 kg/s) were investigated with respect to the set injection angles. Increasing the injection mass flow rate lowers the discharge temperature, pressure, and compression power, as observed in Section 4.4. At the same time, the increase of the injection angle results in the decrease of the under-compression and backflow. For injection of lean solution, it was found that under-compression and backflow occurred with an injected mass flow rate of 0.015 kg/s for injection angles up to 450° and with 0.02 kg/s for injection angles up to 495°. At an injection angle of

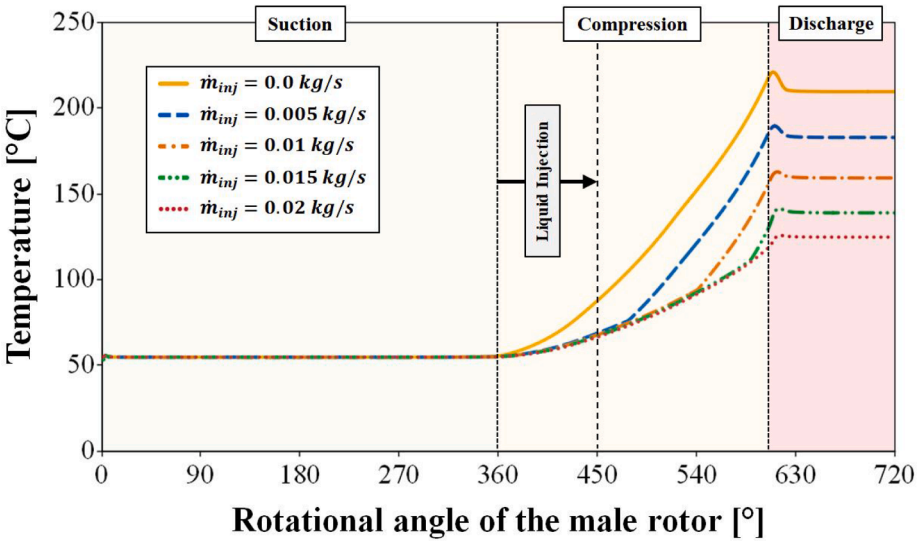

Fig. 8. Temperature evolution for different $\dot{m}_{inj}$ values with $x_{inj} = 0.4$ at constant $C_{leak} = 0.05$ m^{-1} and $\theta_{inj} = 360^{\circ}$.

Table 3
Results for different $\dot{m}_{inj}$ values with $x_{inj} = 0.4$ and 0.7 at constant $C_{leak} = 0.05$ m^{-1} and $\theta_{inj} = 360^{\circ}$.

$\dot{m}_{inj}$ [kg/s]	0.0	0.005	0.01	0.015	0.02
		$x_{inj} = 0.4$			
T_{max} [°C]	221.4	189.9	163.0	141.7	126.0
p_{max} [bar]	27.99	26.76	25.95	25.71	25.55
$\dot{W}_{comp}$ [kW]	58.61	56.04	54.33	53.84	53.49
		$x_{inj} = 0.7$			
T_{max} [°C]	221.4	196.2	173.3	153.3	136.7
p_{max} [bar]	27.99	27.15	26.45	25.95	25.78
$\dot{W}_{comp}$ [kW]	58.61	56.85	55.38	54.33	53.97

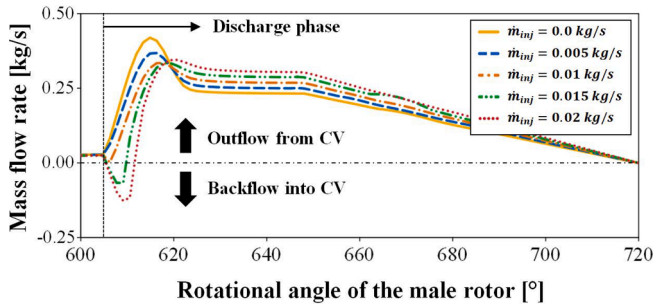

Fig. 9. Mass flow rate evolution for a CV during transition from compression to discharge phase for different $\dot{m}_{inj}$ values with $x_{inj} = 0.4$ at constant $C_{leak} = 0.05$ m^{-1} and $\theta_{inj} = 360^{\circ}$.

540°, no under-compression and backflow were observed. For injection of rich solution, the under-compression and backflow with an injected mass flow rate of 0.015 kg/s occurred only for an injection angle of 360° and with 0.02 kg/s for injection angles up to 450°. More detailed information is presented in Table 4.

The analysis on the provision of wet compression revealed that higher mass flow rates are required for later injection positions. Wet compression was not observed for injection at 540°, while in all other cases sufficient wet compression occurred at injection rates of 0.02 kg/s at the latest. As indicated in Fig. 10 and Table 4, injection at the beginning of the compression phase (360°) shows the best effect on the resulting parameters. However, to ensure continuous wet compression throughout the entire compression phase, larger mass flow rates (min. 0.02 kg/s corresponding to approx. 10 % of the compressor's suction mass flow rate) must be injected. To limit a further increase in the required injection flow rate with the resulting effects such as increased under-compression and backflow, the distribution of the injection over multiple injection ports can be considered, as the single port solution becomes insufficient. Here, a portion of the solution is injected at the beginning of the compression phase at 360°, with the remaining portion injected at a later stage to ensure continuous wet compression for sufficient lubrication and sealing effects.

An investigation with different injection positions (360°, 450° and 495°) and mass flow rates was conducted to evaluate the distribution through two injection ports. The first injection was placed at 360°, the only position capable of ensuring wet compression from the beginning of the compression phase. The second injection port was located either at 450° or 495° to support continuous wet compression towards the end of the compression phase, see Fig. 10. Total injection rates of 0.01 kg/s, 0.015 kg/s and 0.02 kg/s were distributed to both ports with varying injection flow ratios for each port in steps of 0.005 kg/s. The analysis for the case with injection ports located at 360° and 450° revealed that with increasing total injection rate, the discharge temperature, discharge pressure and compressor power decrease, as shown in Table 4. At the same time, the length of the occurring wet compression increases. Increasing the injected flow over the port at 450° (while keeping the total injection flow constant) resulted in slightly increased values for discharge temperature, discharge pressure, and compressor power compared to single port injection (see Table 4). Furthermore, a flattening of the vapor quality curves was accompanied by a lower degree of under-compression and backflow when compared with single port injection and increased injection flow at 360° (two port injection). The analysis for the case with injection ports located at 360° and 495° indicated a similar behaviour with slightly increased values for discharge temperature, discharge pressure and compression power. Unlike the previous case with the second injection at 450°, it is important to note that with a low injection rate of 0.005 kg/s at 360°, no continuous wet compression was achieved with total injection rates of 0.01 kg/s and 0.015 kg/s. Once wet compression stops, it is difficult to regain it at a later stage due to the increased temperature. Therefore, an attempt should be made to ensure continuous wet compression. Based on these results, it is suggested to split the injection over two ports located at 360° and 450°, with the larger proportion of 0.015 kg/s (75 %) injected through the port at 450°. In this case, an injection flow of approx. 0.02 kg/s is still required for complete wet compression. However, the resulting pressure is around 0.01 bar higher, and less under-

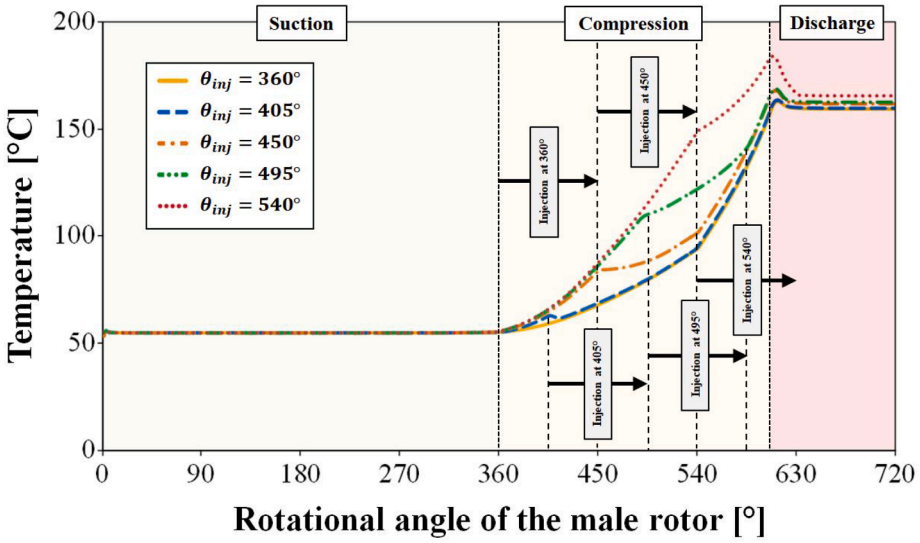

Fig. 10. Example of temperature evolution for different θ_{inj} values with $x_{inj} = 0.4$ at constant $C_{leak} = 0.05\ m^{-1}$ and $\dot{m}_{inj} = 0.01\ kg/s$.

Table 4
Results for different θ_{inj} and $\dot{m}_{inj}$ values with $x_{inj} = 0.4$ and 0.7 at constant $C_{leak} = 0.05\ m^{-1}$.

	$x_{inj} = 0.4$					$x_{inj} = 0.7$				
θ_{inj} [°]	360	405	450	495	540	360	405	450	495	540
					$\dot{m}_{inj} = 0.01$kg/s					
T_{max} [°C]	163.0	163.6	168.2	172.1	184.4	173.3	172.6	177.1	178.1	190.2
p_{max} [bar]	25.95	26.02	26.70	26.78	27.09	26.45	26.49	26.90	26.92	27.22
$\dot{W}_{comp}$ [kW]	54.33	54.49	55.89	56.07	56.71	55.38	55.46	56.31	56.37	57.00
					$\dot{m}_{inj} = 0.015$kg/s					
T_{max} [°C]	141.7	141.5	143.7	147.9	167.1	153.3	154.3	156.6	160.2	175.5
p_{max} [bar]	25.71	25.71	25.83	26.24	26.65	25.95	25.99	26.36	26.49	26.87
$\dot{W}_{comp}$ [kW]	53.84	53.82	54.08	54.94	55.79	54.33	54.42	55.18	55.46	56.25
					$\dot{m}_{inj} = 0.02$kg/s					
T_{max} [°C]	126.0	126.0	126.2	129.3	150.6	136.7	135.8	138.1	142.7	161.2
p_{max} [bar]	25.55	25.56	25.62	25.80	26.23	25.78	25.76	25.84	26.11	26.46
$\dot{W}_{comp}$ [kW]	53.49	53.51	53.63	54.01	54.91	53.97	53.94	54.09	54.67	55.41

compression and backflow will occur.

4.6. Variation of compressor speed

In the intended operation of a compressor in the ACHP system, the compressor speed will vary depending on the required operating condition. As outlined in a review by Wang et al. [18], investigations in the literature show that changes in speed affect the different performance parameters of the compressor. To gain a better understanding of the achievable performance parameters at varying operating points of the compressor, the influence of the operational frequency was investigated. The operational frequency was set to 62.5 Hz (125 %), 50 Hz (100 %), 37.5 Hz (75 %) and 25 Hz (50 %) with a constant C_{leak} value of 0.05 m^{-1} and single-port injection at an injection angle of 360°. The liquid injection rate with respect to the specific compressor suction mass flow rate was varied from 0 %, 5 %, and 10 %, with NH_3 mass fractions of 0.4 and 0.7.

The suction mass flow rate of the compressor for the ideal case without leakage ($C_{leak} = 0.0\ m^{-1}$) and no liquid injection ($\dot{m}_{inj}$ set to 0) increases linearly with increasing operational frequency. Under consideration of internal leakage ($C_{leak} = 0.05\ m^{-1}$), the results revealed that a decrease in the operational frequency causes an increase in the occurring leakage flow. Due to reduced rotor speed, the residence time of the working fluid in the cavity volume during the compression process is extended, and leakages increase. Fig. 11 presents the achieved volumetric efficiencies compared to the reference case without leakage for

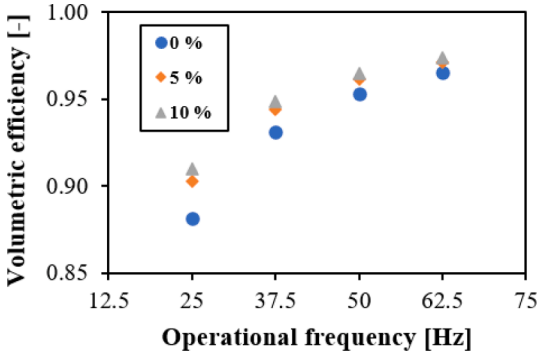

Fig. 11. Volumetric efficiency for varying f and liquid injection flow rates from 0 %, 5 % and 10 % with $x_{inj} = 0.4$ at constant $C_{leak} = 0.05\ m^{-1}$ and $\theta_{inj} = 360°$.

the investigated operational frequencies and liquid injection flow rates corresponding to 0 %, 5 % and 10 % of the respective suction mass flow rates.

The results demonstrate that the volumetric efficiency increases for higher operational frequencies. Moreover, the increase in the injection rate provides an improvement in the volumetric efficiency at constant frequencies. Here, the difference from 0 % to 5 % is larger than from 5 % to 10 %, indicating that the liquid has a positive effect on the occurring leakages, although there is a maximum possible value that can be

achieved.

The same trends are observed for the other investigated parameters. The maximum temperature reached decreases for increasing operational frequencies from 238.9 °C at 25 Hz to 218.3 °C at 62.5 Hz with no injection. When the injection rates are increased to 5 %, both the respective temperatures and the total variation decrease (174.1 °C at 25 Hz and 161.6 °C at 62.5 Hz). At an injection rate of 10 %, full wet compression is achieved for all cases studied, and the temperatures are greatly reduced to 130.5 °C at 25 Hz and 125.8 °C at 62.5 Hz. Therefore, to obtain the same temperature as in cases with higher operational frequency, a higher injection ratio is required. The same beneficial impact of the injection is observed for the changes in the maximum pressure (from 28.08 bar to 26.14 bar to 25.71 bar at 62.5 Hz and from 27.53 bar to 25.61 bar to 25.24 bar at 25 Hz), and the maximum required compression power (from 73.79 kW to 68.42 kW to 67.28 kW bar at 62.5 Hz and from 28.82 kW to 26.81 kW to 26.42 kW at 25 Hz), with the lowest values are obtained with 10 % injection rate.

The determination of isentropic and adiabatic efficiency for the comparison and evaluation of the achieved efficiency is complicated in the present study. Due to the liquid injection, a continuous heat transfer takes place, which is often solved by splitting the compression process, as described by Tian et al. [22] and Di et al. [43]. However, the NH_3 mass fraction also changes continuously, complicating the calculation and making comparison difficult. For this reason, the specific power is calculated as the ratio of the maximum total compression power to the suction mass flow rate. Fig. 12 shows the determined specific power for the investigated operational frequencies and liquid injection flow rates corresponding to 0 %, 5 % and 10 % of the respective suction mass flow rates.

The results indicate that the specific power required for compression decreases as the operational frequency increases. In addition, a higher injection rate ensures a further reduction in specific power. Here, the characteristics are similar to the previously described trends. It can be concluded that the injection rate and ratio must be adapted and controlled according to the compressor speed. These observations are consistent with the results presented in the literature by various authors such as Tian et al. [22], Wang [39] and Li et al. [44].

4.7. Discussion of results and model limitations

The results and model limitations are discussed with respect to the conducted investigation of the liquid injection for an oil-free twin screw compressor within the ACHP system. The objective of the developed MODELICA screw compressor model was to improve the understanding of thermodynamic behaviour during the compression process using NH_3-H_2O mixture as refrigerant and liquid injection with varying NH_3 mass fractions. The preliminary analysis indicated that both desorption of ammonia from the liquid phase and full evaporation are achievable,

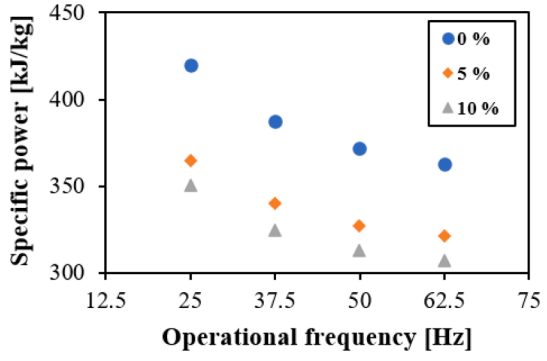

Fig. 12. Specific power (compression power to compressed working fluid flow) for varying f and liquid injection flow rates from 0 %, 5 % and 10 % with x_{inj} = 0.4 at constant C_{leak} = 0.05 m^{-1} and θ_{inj} = 360°.

irrespective of the subcooled state of the injected lean or rich solution.

The developed model consists of moving control volumes containing the working fluid in liquid vapor equilibrium and performing the compression process without mechanical losses. To consider occurring leakages across the rotor tips and housing, a function was implemented, and a leakage coefficient (C_{leak}) was defined. The analysis with different values indicated the influence on the pressure evolution and resulting over- or under-compression. A suitable value of 0.05 m^{-1} was selected for the further investigation to also consider additional losses of other leakage paths. Heat losses to the compressor body and ambient were not considered for further investigations after assessing their influence.

The study of the NH_3 mass fraction revealed that a reduction in the ammonia content resulted in decreasing values for discharge temperature, discharge pressure and compression power at a constant injection mass flow rate. It was demonstrated that the presence and duration of wet compression (for lubrication and sealing of the compressor) are a function of the NH_3 mass fraction of the injected solution. The best results were obtained with pure water, and it is therefore preferable to inject a solution with low NH_3 mass fraction, such as the lean solution in the ACHP system.

The investigation of the injection mass flow rates demonstrated that wet compression throughout the whole compression phase is possible with an increase in the injection quantity. However, if the injection flow becomes too large, negative effects such as under-compression and backflow from the discharge port will occur. At constant injection flow rates, these effects are less significant with an increased NH_3 mass fraction. An optimum of 0.01 kg/s for the lean solution and between 0.01 kg/s and 0.015 kg/s for the rich solution was determined.

The positioning of injection ports revealed a strong influence on the results obtained. Wet compression was observed with an injection flow of 0.01 kg/s for injection at 360° and 405°. However, this did not occur for the entire compression phase. For this injection rate, no under-compression or backflow was observed for both lean and rich solution. To achieve complete wet compression, larger injection flows up to 0.02 kg/s are required, corresponding to approx. 10 % of the compressor's suction mass flow. At the same time, the provision of complete wet compression through the injection at 360° with 0.02 kg/s led to the highest under-compression and backflow from the discharge port. The split of two injection ports was investigated to evaluate further options to ensure continuous wet compression. It was found that injection at 360° and 450° with a higher injection rate of 0.015 kg/s (75 % of total injection) at 450° leads to higher pressures of 0.01 bar with a reduction in occurring under-compression and backflows. The analysis of varying compressor speed revealed that leakage flows increase at reduced operational frequency. This results in an increased temperature and higher required liquid quantities. It can be concluded that the injection rate must be adapted to the respective operating conditions.

For the comprehensive evaluation of the obtained results, the given model limitations are addressed and discussed. Occurring leakages, mechanical and heat losses, and other component and/or operation specific parameters are difficult to predict without detailed geometry and data and often require experimental investigations. The implemented model of leakage allows to understand and adjust different leakage paths and their geometries. At the same time, the absence of a specific liquid film due to the homogeneous vapor–liquid equilibrium approach of each CV hampers the accurate determination of occurring leakage flows and achievable efficiencies. Since the compressor efficiencies were not a primary concern in this study, the assumption of 100 % mechanical efficiency is reasonable. However, this assumption neglects the fact that mechanical losses under real conditions can influence the temperature evolution of the working fluid by generating heat and thus effect all other operational parameters. This may be compensated for to some extent, as additionally counteracting heat losses to the compressor body were not considered.

The solution is injected in a highly supercooled state and the time to achieve eventual liquid–vapor equilibrium becomes extremely limited

due to the high rotational speeds and relatively short residence time. Furthermore, the liquid–vapor surface area is further reduced due to imperfect dispersion without the use of atomizing nozzles or similar devices. Forces resulting from the rotational motion of the rotors cause the liquid droplets to move toward the rotor tips and/or the compressor housing, which impedes uniform dispersion. All these factors can hamper substantial heat and mass transfer under real operating conditions, resulting in the presence of simultaneously remaining liquid in the CV despite superheated vapor being present. Compared to this, the assumption of liquid–vapor equilibrium with homogeneous distribution in the CV can lead to an overestimation of the pressure and an underestimation of the temperature evolution. Due to these known limitations and further unknown uncertainties, the results are considered as a kind of best-case analysis.

5. Conclusion

The objective of this study was to develop an oil-free twin screw compressor model with NH_3-H_2O mixture as refrigerant and liquid injection to improve the understanding of thermodynamic behaviour during the compression process and to discuss the integration into the ACHP system. The preliminary thermodynamic analysis indicated that both desorption of ammonia from the liquid phase and full evaporation are achievable during the compression process with liquid injection, irrespective of the subcooled state of the injected lean or rich solution. For a comprehensive investigation, a quasi-one-dimensional numerical model was developed using the Modelica language that considers the effects of liquid injection, leakage flows, and heat losses. The model was designed to investigate various arrangements of liquid injection and operating conditions and consists of eight control volumes moving in a continuous compression cycle, containing the working fluid in liquid vapor equilibrium. It is suitable for both transient and steady-state analysis and was used to study the effects of varying NH_3 mass fractions, injection amounts and injection positions during the compression process.

The analysis of the obtained results revealed a strong influence of the investigated parameters on the compression process and the evolution of temperature, pressure, and compression power.

- For the application in the ACHP system, it was concluded that the injection of solution with a low NH_3 mass fraction (see Fig. 1 - Option 1: Injection of lean solution) should be preferred. It was observed that a lower NH_3 mass fraction resulted in decreased discharge temperature, discharge pressure, and compression power. The lowest values were obtained for the injection of pure water. High temperature is generally beneficial for oil-free high temperature heat pumps; however, it can be limited by the material properties of the compressor.
- With the injection of 0.01 kg/s (about 5 % of the compressor's suction mass flow rate) of lean solution, the temperature was sufficiently reduced, and the pressure evolution was adapted to the externally applied pressure ratio. Thereby, under-compression and backflow from the discharge were minimized, which is important for the efficient and sustainable operation of the compressor.
- Wet compression was observed during the injection at the beginning of compression but was not continuous throughout the entire compression phase. To ensure a continuous liquid film that provides sufficient lubrication and sealing throughout the compression process, the injection rate must be increased to about 10 % of the compressor's suction mass flow rate (0.02 kg/s).
- When injecting through a single port, full wet compression was observed only when injected at 360° (at the beginning of the compression phase), regardless of the injection rate. Thus, the placement of one port at 360° is important for ensuring a continuous liquid film.
- To further optimize the achievable results, injection through an additional port in the mid-compression phase (450° or 495°) was investigated. Compared to the single-port injection, the distribution over two injection ports, with the smaller portion (approx. 25 %) injected at 360° at the beginning of the compression process and the greater portion (approx. 75 %) injected at 450°, can support the provision of wet compression and reduce occurring under-compression.
- An investigation with varying compressor speed revealed the influence on the investigated compressor parameters. It was concluded that the injection rate and ratio must be adjusted and controlled to achieve identical temperatures depending on the operating point.

The limitations of the existing model due to the assumptions for the working fluid in each control volume with homogeneous behaviour and liquid vapor equilibrium, as well as the simplified representation of leakage paths and other losses were discussed. Due to these known limitations and further unknown uncertainties, the results are considered as a kind of best-case analysis. However, the conducted investigation fulfils the purpose to provide information about the expected behaviour and the preferred integration into ACHP systems. Furthermore, it provides results for the lowest required injection mass flow and the distribution of injection positions to improve the planning of necessary experimental investigations. The adaptability of the model also provides a comparatively simple increase in the degree of detail for further investigations.

Further research will focus on the experimental investigation and realization of oil-free operation by lubricating and cooling the bearings with the injected solution. This can be supported by a comprehensive life cycle assessment to investigate how the use of more specialized materials like oil-free bearings and more advanced sealings compares to a potential complete elimination of lubrication oil and oil separation equipment. Furthermore, an exergy analysis can be conducted to investigate the influence on the overall ACHP system performance.

Declaration of Competing Interest

The authors declare that they have no known competing financial interests or personal relationships that could have appeared to influence the work reported in this paper.

Data availability

Data will be made available on request.

Acknowledgements

This publication has been funded by HighEFF - Centre for an Energy Efficient and Competitive Industry for the Future, an 8-years' Research Centre under the FME-scheme (Centre for Environment-friendly Energy Research, 257632). The authors gratefully acknowledge the financial support from the Research Council of Norway and user partners of HighEFF.

References

[1] International Energy Agency, Energy Efficiency 2018: Analysis and outlooks to 2040, 2018. Available from: <https://www.iea.org/reports/energy-efficiency-2018>.
[2] International Energy Agency, Net Zero by 2050 - A Roadmap for the Global Energy Sector, 2021. Available from: <https://www.iea.org/reports/net-zero-by-2050>.
[3] E. Woolley, Y. Luo, A. Simeone, Industrial waste heat recovery: a systematic approach, Sustain. Energy Technol. Assessments 29 (2018) 50–59, https://doi.org/10.1016/j.seta.2018.07.001.
[4] M. Papapetrou, G. Kosmadakis, A. Cipollina, U. La Commare, G. Micale, Industrial waste heat: estimation of the technically available resource in the EU per industrial sector, temperature level and country, Appl. Therm. Eng. 138 (2018) 207–216, https://doi.org/10.1016/j.applthermaleng.2018.04.043.

[5] R. Bergamini, J.K. Jensen, B. Elmegaard, Thermodynamic competitiveness of high temperature vapor compression heat pumps for boiler substitution, Energy 182 (2019) 110–121, https://doi.org/10.1016/j.energy.2019.05.187.
[6] M.U. Ahrens, S.S. Foslie, O.M. Moen, M. Bantle, T.M. Eikevik, Integrated high temperature heat pumps and thermal storage tanks for combined heating and cooling in the industry, Appl. Therm. Eng. 189 (2021) 10, https://doi.org/10.1016/j.applthermaleng.2021.116731.
[7] C. Arpagaus, F. Bless, M. Uhlmann, J. Schiffmann, S.S. Bertsch, High temperature heat pumps: market overview, state of the art, research status, refrigerants, and application potentials, Energy 152 (2018) 985–1010, https://doi.org/10.1016/j.energy.2018.03.166.
[8] G. Kosmadakis, Estimating the potential of industrial (high-temperature) heat pumps for exploiting waste heat in EU industries, Appl. Therm. Eng. 156 (2019) 287–298, https://doi.org/10.1016/j.applthermaleng.2019.04.082.
[9] A. Marina, S. Spoelstra, H.A. Zondag, A.K. Wemmers, An estimation of the European industrial heat pump market potential, Renew. Sustain. Energy Rev. 139 (2021), 110545, https://doi.org/10.1016/j.rser.2020.110545.
[10] J. Jiang, B. Hu, R.Z. Wang, N. Deng, F. Cao, C.-C. Wang, A review and perspective on industry high-temperature heat pumps, Renew. Sustain. Energy Rev. 161 (2022), 112106, https://doi.org/10.1016/J.RSER.2022.112106.
[11] J.K. Jensen, W.B. Markussen, L. Reinholdt, B. Elmegaard, On the development of high temperature ammonia-water hybrid absorption-compression heat pumps, Int. J. Refrig. 58 (2015) 79–89, https://doi.org/10.1016/j.ijrefrig.2015.06.006.
[12] M.U. Ahrens, M. Loth, I. Tolstorebrov, A. Hafner, S. Kabelac, R. Wang, T. M. Eikevik, Identification of existing challenges and future trends for the utilization of ammonia-water absorption-compression heat pumps at high temperature operation, Appl. Sci. 11 (2021) 4635, https://doi.org/10.3390/app11104635.
[13] D. Zaytsev, Development of wet compressor for application in compression-resorption heat pumps, Technische Universiteit Delft, 2003. Available from: <http://repository.tudelft.nl/view/ir/uuid%3Aca640a9d-6fe1-4a59-b42c-594213703f07/>.
[14] J. Shen, Z. Xing, K. Zhang, Z. He, X. Wang, Development of a water-injected twin-screw compressor for mechanical vapor compression desalination systems, Appl. Therm. Eng. 95 (2016) 125–135, https://doi.org/10.1016/j.applthermaleng.2015.11.057.
[15] C.A. Infante Ferreira, C. Zamfirescu, D. Zaytsev, Twin screw oil-free wet compressor for compression-absorption cycle, Int. J. Refrig. (2006), https://doi.org/10.1016/j.ijrefrig.2005.10.006.
[16] D. Zaytsev, C.A. Infante Ferreira, Screw compressor for ammonia-water heat pump lubricated by the process mixture, in: Int. Compress. Eng. Conf. Sch., 2002.
[17] M.A. Heiyanthuduwage, S. Mounoury, A. Kovacevic, Performance prediction methods for screw compressors, in: 7th Int. Conf. Compressors Their Syst. 2011, Woodhead Publishing Limited, London, 2011, pp. 411–420, doi: 10.1533/9780857095350.8.411.
[18] C. Wang, B. Wang, M. Liu, Z. Xing, A review of recent research and application progress in screw machines, 10 (2022) 62, doi: 10.3390/MACHINES10010062.
[19] N. Stošic, L. Milutinović, K. Hanjalić, A. Kovačević, Investigation of the influence of oil injection upon the screw compressor working process, Int. J. Refrig. 15 (1992) 206–220, https://doi.org/10.1016/0140-7007(92)90051-U.
[20] N. Stosic, I.K. Smith, A. Kovacevic, Estimation and control of heat transfer in screw compressor rotors, in: Proc. IMECE04, 2004 ASME Int. Mech. Eng. Congr. Expo., Anaheim, 2004, pp. 441–446, doi: 10.1115/IMECE2004-60516.
[21] Q. Yang, C. Liu, Q. Zhang, G. Liu, Y. Zhao, L. Li, Experimental investigation of the water-injected process-gas screw compressor, J. Process Mech. Eng. 232 (2018) 3–11, https://doi.org/10.1177/0954408916666573.
[22] Y. Tian, J. Shen, C. Wang, Z. Xing, X. Wang, Modeling and performance study of a water-injected twin-screw water vapor compressor, Int. J. Refrig. 83 (2017) 75–87, https://doi.org/10.1016/j.ijrefrig.2017.04.008.
[23] N. Basha, A. Kovacevic, S. Rane, Numerical investigation of oil injection in screw compressors, Appl. Therm. Eng. 193 (2021), 116959, https://doi.org/10.1016/J.APPLTHERMALENG.2021.116959.
[24] Y. Tian, H. Yuan, C. Wang, H. Wu, Z. Xing, Numerical investigation on mass and heat transfer in an ammonia oil-free twin-screw compressor with liquid injection, Int. J. Therm. Sci. (2017), https://doi.org/10.1016/j.ijthermalsci.2017.06.007.
[25] H.H. Patel, V.J. Lakhera, A critical review of the experimental studies related to twin screw compressors, J. Process Mech. Eng. 234 (2020) 157–170, https://doi.org/10.1177/0954408919869534.
[26] V. Gudjonsdottir, C.A. Infante Ferreira, A. Goethals, Wet compression model for entropy production minimization, Appl. Therm. Eng. 149 (2019) 439–447, https://doi.org/10.1016/j.applthermaleng.2018.12.065.
[27] V. Gudjonsdottir, C.A. Infante Ferreira, Technical and economic analysis of wet compression–resorption heat pumps, Int. J. Refrig. 117 (2020) 140–149, https://doi.org/10.1016/j.ijrefrig.2020.05.010.
[28] A. Osenbrück, Verfahren zur Kälteerzeugung bei Absorptionsmaschinen, DPR 84084, 1895.
[29] N.S. Ganesh, T. Srinivas, Evaluation of thermodynamic properties of ammonia-water mixture up to 100 bar for power application systems, J. Mech. Eng. Res. 3 (2011) 25–39.
[30] M. Chamoun, R. Rulliere, P. Haberschill, J.L. Peureux, Modelica-based modeling and simulation of a twin screw compressor for heat pump applications, Appl. Therm. Eng. (2013), https://doi.org/10.1016/j.applthermaleng.2013.04.020.
[31] Dassault Systems, DYMOLA Systems Engineering: Multi-Engineering Modeling and Simulation based on Modelica and FMI, 2022. Available from: <https://www.3ds.com/products-services/catia/products/dymola/>.
[32] TLK-Thermo GmbH, TIL Suite – Simulates thermal systems, 2022. Available from: <https://www.tlk-thermo.com/index.php/en/software/til-suite>.
[33] TLK-Thermo GmbH, TILMedia Suite – Software package for calculating the properties of thermophysical substances, 2022. Available from: <https://www.tlk-thermo.com/index.php/en/software/tilmedia-suite>.
[34] M.U. Ahrens, E.K. Tønsberg, I. Tolstorebrov, A. Hafner, T.M. Eikevik, Modelling approach for a liquid-injected ammonia-water screw compressor, in: 10th IIR Conf. Compressors Refrig., Bratislava, 2021, pp. 13–15, doi: 10.18462/iir.compr.2021.0385.
[35] A. Bejan, Advanced Engineering Thermodynamics, 4th ed., John Wiley & Sons, Inc., 2016, doi: 10.1002/9781119245964.
[36] N. Stosic, I.K. Smith, A. Kovacevic, Optimisation of screw compressors, Appl. Therm. Eng. 23 (2003) 1177–1195, https://doi.org/10.1016/S1359-4311(03)00059-0.
[37] J. Li, H. Wu, B. Wang, Z. Xing, P. Shu, Research on the performance of water-injection twin screw compressor, Appl. Therm. Eng. 29 (2009) 3401–3408, https://doi.org/10.1016/J.APPLTHERMALENG.2009.05.018.
[38] W. Huagen, X. Ziwen, S. Pengcheng, Theoretical and experimental study on indicator diagram of twin screw refrigeration compressor, Int. J. Refrig. 27 (2004) 331–338, https://doi.org/10.1016/J.IJREFRIG.2004.01.004.
[39] C. Wang, Z. Xing, W. Chen, S. Sun, Z. He, Analysis of the leakage in a water-lubricated twin-screw air compressor, Appl. Therm. Eng. 155 (2019) 217–225, https://doi.org/10.1016/j.applthermaleng.2019.04.001.
[40] M.G. Read, I.K. Smith, N. Stosic, Influence of rotor geometry on tip leakage and port flow areas in gerotor-type twin screw compressors, Proc. Inst. Mech. Eng. Part E J. Process Mech. Eng. 236 (1) (2022) 94–102.
[41] J.S. Fleming, Y. Tang, The analysis of leakage in a twin screw compressor and its application to performance improvement, Proc. Inst. Mech. Eng. Part E J. Process Mech. Eng. 209 (2) (1995) 125–136.
[42] S. Smitt, I. Tolstorebrov, A. Hafner, Performance improvement of integrated CO2 systems with HVAC and hot water for hotels, Therm. Sci. Eng. Prog. 23 (2021), https://doi.org/10.1016/J.TSEP.2021.100869.
[43] D. Wu, J. Jiang, B. Hu, R.Z. Wang, Experimental investigation on the performance of a very high temperature heat pump with water refrigerant, Energy 190 (2020), 116427, https://doi.org/10.1016/j.energy.2019.116427.
[44] Y. Li, J. Wang, Y. Wu, B. Lei, R. Zhi, L. Shen, Influence of water injection parameters on the performance of a water-lubricated single-screw air compressor, J. Mech. Sci. Technol. 36 (2022) 445–456, doi: 10.1007/S12206-021-1242-4.